Indium joints for cryogenic gravitational wave detectors

OPEN ACCESS
IOP Publishing
Classical and Quantum Gravity
Class. Quantum Grav. **32** (2015) 245013 (18pp)
doi:10.1088/0264-9381/32/24/245013

Indium joints for cryogenic gravitational wave detectors

G Hofmann[1], D Chen[2], G Bergmann[3], G D Hammond[4], M Hanke[3], K Haughian[4], D Heinert[1], J Hough[4], A Khalaidovski[2], J Komma[1], H Lück[3], E Majorana[5], M Masso Reid[4], P G Murray[4], L Naticchioni[5], R Nawrodt[1], S Reid[6], S Rowan[4], F Schmidl[1], C Schwarz[1], P Seidel[1], T Suzuki[7], T Tomaru[7], D Vine[6] and K Yamamoto[2]

[1] Institut für Festkörperphysik, Friedrich-Schiller-Universität Jena, Helmholtzweg 5, D-07743 Jena, Germany
[2] Institute for Cosmic Ray Research (ICRR), The University of Tokyo, 5-1-5, Kashiwanoha, Kashiwa, Chiba, 277-8582, Japan
[3] Max Planck Institute for Gravitational Physics (Albert Einstein Institute) and Institut fr Gravitationsphysik, Leibniz Universität Hannover, Callinstr. 38, D-30167 Hannover, Germany
[4] SUPA, School of Physics and Astronomy, Institute for Gravitational Research, University of Glasgow, Glasgow G12 8QQ, UK
[5] INFN, Sezione di Roma 1, I-00185 Rome, Italy
[6] SUPA, University of the West of Scotland, Paisley PA1 2BE, UK
[7] High Energy Accelerator Research Organization (KEK), 1-1 Oho, Tsukuba, Ibaraki, 305-0801, Japan

E-mail: yamak@icrr.u-tokyo.ac.jp

Received 19 August 2015, revised 24 September 2015
Accepted for publication 12 October 2015
Published 3 December 2015

Abstract

A viable technique for the preparation of highly thermal conductive joints between sapphire components in gravitational wave detectors is presented. The mechanical loss of such a joint was determined to be as low as 2×10^{-3} at 20 K and 2×10^{-2} at 300 K. The thermal noise performance of a typical joint is compared to the requirements of the Japanese gravitational wave detector, KAGRA. It is shown that using such an indium joint in the suspension system allows it to operate with low thermal noise. Additionally, results on the maximum amount of heat which can be extracted via indium

joints are presented. It is found that sapphire parts, joined by means of indium, are able to remove the residual heat load in the mirrors of KAGRA.

Keywords: KAGRA, gravitational wave detector, gravitational waves, sapphire, indium, cryogenic

(Some figures may appear in colour only in the online journal)

1. Introduction

The detection of gravitational waves is one of the most challenging tasks in astrophysics today. Although they have already been verified indirectly, the direct detection of these waves has still not been achieved. Today's most promising detectors are based on a Michelson interferometer using optical components in pendulum suspensions as free falling test masses. These instruments have already reached a sensitivity for length changes of better than 10^{-18} m [1–4]. Several science runs have been made, taking data in joint operation schemes over many weeks. However, a direct detection of a gravitational wave has so far not been possible though upper limits on astrophysical parameters of possible sources could be given [5–9]. Currently, these detectors have been, or are about to be, upgraded to the so-called second or advanced generation. Advanced detectors, like Advanced LIGO [2] and Advanced Virgo [10], use quasi-monolithic suspensions based on fused silica elements joined by welding [11–13] and hydroxide catalysis bonding [14] to reduce suspension thermal noise which limits the sensitivity in the low frequency band. Additionally, novel techniques like signal recycling [15, 16], higher laser power [17] or squeezed light [18] are being used to reduce further the noise limit throughout the whole detection band. Many of these techniques have been demonstrated already in GEO600 [19–21]. The design sensitivity of the advanced detectors aims to produce a tenfold reduction of noise throughout the detection band compared to the first generation.

The Japanese gravitational wave detection project KAGRA [22–24] adds two additional features to the list of improvements. It will be the first advanced detector being operated underground in order to reduce seismic disturbances and it will be the first km scale interferometric gravitational wave detector which will use optics cooled to cryogenic temperatures of about 20 K. Operating the detector at low temperatures will greatly reduce thermal noise [25, 26] as well as thermal lensing problems [27]. Unfortunately, operating at cryogenic temperatures does not allow for the use of fused silica as a test mass or as a suspension material due to its large mechanical loss at low temperatures [28–31] and its poor thermal conductivity at cryogenic temperatures [32, 33]. Both originate in the glassy structure of this material. An alternative is to use crystalline materials [25, 34]. Several materials have been proposed and investigated in the past for future gravitational wave detectors, amongst them sapphire [35–37], calcium fluoride [38–40] and silicon [41–43]. Sapphire has been chosen to be the baseline material for the cryogenic operation of KAGRA while silicon is a potential candidate material for a third generation detector in Europe called the Einstein Telescope [23, 44].

In order to construct a quasi-monolithic suspension from crystalline materials it is necessary to develop a fabrication technique for the fibres, a suitable jointing technique for the components, as well as to check if the techniques being used are compliant with the thermal noise and also the heat removal requirements. It was shown [45–48] that hydroxide catalysis bonding—developed initially for the Gravity Probe B mission [49] and successfully applied

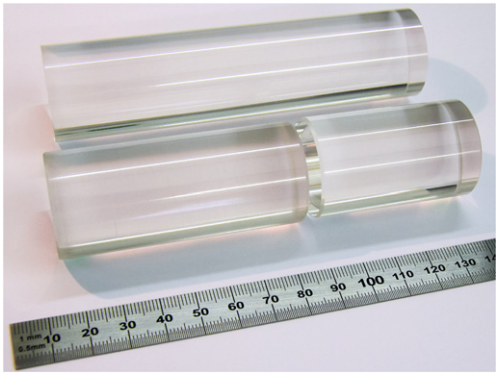

Figure 1. The two sapphire cylinders of 70 mm and 50 mm length at the bottom were jointed by indium to form one sample. The mechanical loss of the indium jointing layer is extracted via comparison to the reference sample at the top of the same dimensions and at the same temperatures.

to room temperature suspensions [14, 50–52]—can be used to form strong bonds between sapphire pieces.

In case of a necessary repair, neither standard debonding routines nor welding techniques exist so far that could be used for the crystalline suspension elements. Strong research to overcome this issue is currently underway. Thus it has been proposed that thin indium layers be used as a jointing material between sapphire components which can be disassembled easily in the case of a failure in the suspension system. Depending on the joint strength, parts can be pulled apart with or without additional heating or an acid (e.g. nitric acid) can be used to dissolve the joints. Possible indium joints have been studied in the past for several applications and have been suggested for use in gravitational wave detectors [53, 54]. In the case of the KAGRA detector, the suspension is proposed to be assembled using different bonding techniques (e.g. hydroxide catalysis bonding for attachments to the test mass, indium for compression joints between the fibres and the blade springs).

Here, techniques to join sapphire components by means of indium layers are presented. These techniques are straightforward and easy to use and therefore they can be used on site for KAGRA. The mechanical loss of such an indium joint is investigated and a first estimate of the overall thermal noise of a suspension using this technique is given. Additionally, a measurement is presented which confirms the capability of this jointing technique to produce highly thermal conductive components which are able to handle the heat load from residual optical absorption of the test masses in KAGRA.

2. Sample preparation and indium jointing process

Several techniques are discussed in the literature for jointing parts by means of indium [55]. One of the major obstacles is the formation of a thin protective oxide layer on the indium surface. This oxide layer lowers the adhesion of the indium on sapphire and supports the dewetting process. Thus weakening of the joint will be unavoidable. However, the joints which were prepared for the experimental determination of the mechanical loss were revealed to be strong enough for handling and measuring. In the case of KAGRA, a purely compressive design for the indium joint has been proposed so the strength of the joint plays a role

only during the handling and assembling of the system and is not seen as an issue during operation.

2.1. Sample overview

All the single crystal sapphire samples were obtained from Impex [56]. Two cylindrical shaped samples, each 30 mm in diameter and 50 mm and 70 mm in length, respectively, are used for the mechanical loss measurement of the indium joint (figure 1). Another sapphire cylinder of the same diameter but of 120 mm length serves as the non-jointed reference and is used for comparison (figure 1). The axis of all the cylinders is coincident with the crystallographic *c*-axis. The surfaces are inspection polished, except the two surfaces of the shorter cylinders intended for jointing which are polished to a global peak to valley flatness of $\lambda/10$ ($\lambda = 632.8$ nm).

The bar shaped samples used to check the heat extraction measure 50 mm in length and have a cross section of 5 mm $\times$ 5 mm. One end of each bar was polished to $\lambda/10$ to allow for a proper jointing while all the remaining surfaces were left ground. Again the *c*-axis is aligned along the bar.

2.2. Cleaning of samples

In general, all samples have been cleaned in several steps. In the first step nitric acid (typically 25 % solution to avoid hazardous reactions with possible organic contaminants) was used to remove any possible remaining indium from previous tests. In the second step a mixture of sulphuric acid and hydrogen peroxide solution has been used to remove organic contamination (finger prints, vacuum grease from previous measurements, etc.). After that a common RCA clean was applied [57, 58] (for details see appendix C). Finally the samples were blown dry by means of high purity nitrogen.

Initial steps also involved different acids (e.g. formic acid, nitric acid, hydrochloric acid) to remove the oxide layer from the indium before the jointing process. This procedure was done in a glove box using argon or nitrogen as a protective atmosphere. However, any remaining small amounts of oxygen resulted in the oxide layer quickly forming again. Therefore it was not even possible to produce pure indium surfaces which could be handled for a few minutes in order to form the indium joint. For the formation of the joints on site at the KAGRA detector, in particular, it will not be possible to avoid the natural growth of indium oxide at the surface. Thus all jointing tests presented here were done using indium with a native oxide layer.

2.3. Indium jointing techniques

Indium foils of 100 μm thickness and a purity of 99.999% were obtained from Advent Research Materials. The foil was prepared in diluted hydrochloric acid to remove the old oxide layer prior to being placed between the samples. This ensures that only a thin and fresh native oxide layer of a few nm is incorporated in the jointing process. The indium foil was placed between the two cylinders which were aligned visually along the axis while any further crystal orientation was left unconsidered.

Additional weight of 1.5 kg was put on top of the cylinder stack, giving a total weight of 1.7 kg, equivalent to a pressure of 23.6 kPa on the joint. In previous test runs this pressure turned out to ensure the layer became thin enough without squeezing out all the indium during heating. Heat was applied from the bottom using a hot plate at a temperature of 200 °C. A temperature sensor was fixed on the upper sample to ensure a reasonable temperature to melt

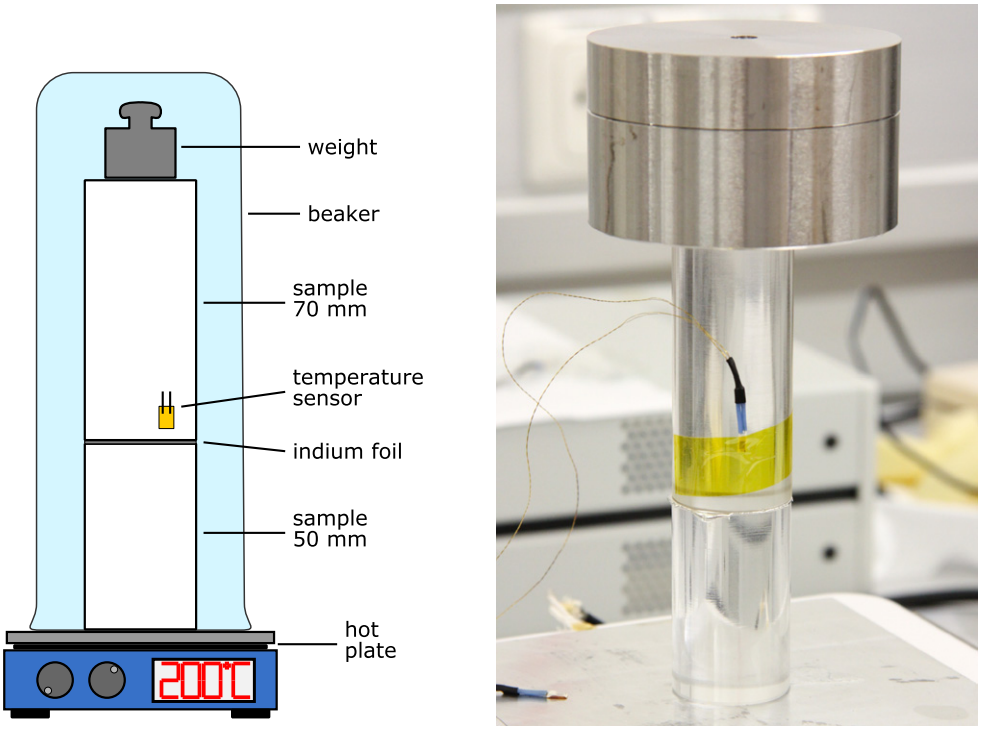

Figure 2. (a) Schematic drawing and (b) photograph of the indium jointing procedure. A hot plate was used to melt the indium foil between the sapphire cylinders. A temperature sensor was fixed on the upper sample to control the temperature. A weight was put on top to obtain a thin indium layer.

the indium foil in between at around 156.6 °C. A glass beaker wrapped with aluminium foil covered the samples to concentrate the heat (see figure 2). The beaker was purged with high purity nitrogen to avoid a further oxidation of the indium during the jointing process. The temperature was kept constant for 2 h before the hot plate was switched off and the whole setup was allowed to cool down to room temperature overnight. Indium protruding around the joint was removed. The whole process was carried out in a dust-free environment but non-clean-room conditions.

The indium layer between both samples turned out to be semi-transparent and porous but still mechanically robust. The photograph of the indium layer shown in figure 3(a) was converted into a black and white image. The ratio of black and white pixels was used to determine the surface coverage to be $(40 \pm 10)\,\%$. The thickness of the indium layer was obtained in a side view via comparison with a micrometer stage, using a microscope. It was determined to be $(8.4 \pm 2.0)\,\mu$m. This error occurs due to a variation of the layer thickness around the circumference.

A second bonding was carried out exactly as described above except that both sapphire surfaces intended for bonding were covered by 0.5 μm of indium via thermal evaporation prior to the indium foil being inserted. This helped to reduce the effect of dewetting and thus, with previously coated surfaces, the bond layer appears quite dense with a coverage of about

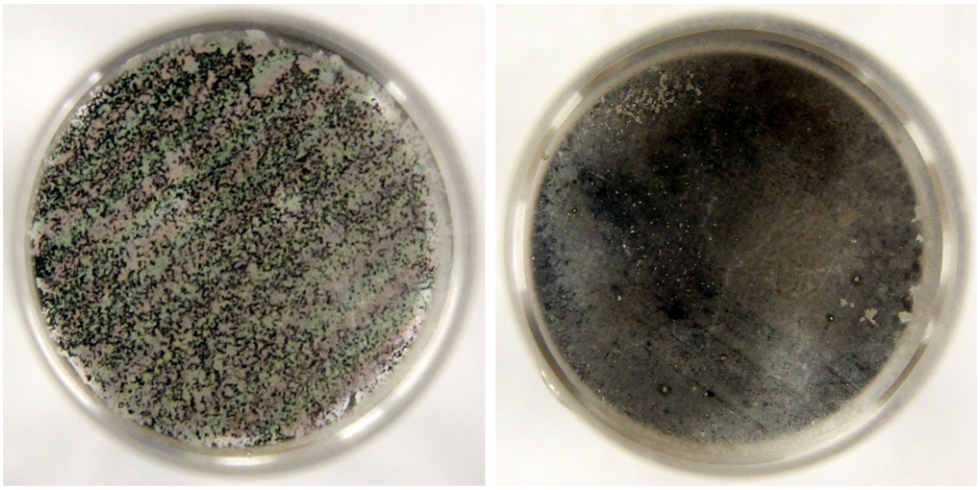

(a) (b)

Figure 3. Photographs of the indium layers between the sapphire samples taken along the cylinder axis. (a) Analysis of the slightly porous indium layer reveals a coverage of (40 ± 10) % using only the indium foil for jointing. (b) The nearly compact layer with (95 ± 5) % of the jointing surface covered is obtained for previously indium film coated surfaces prepared by thermal evaporation.

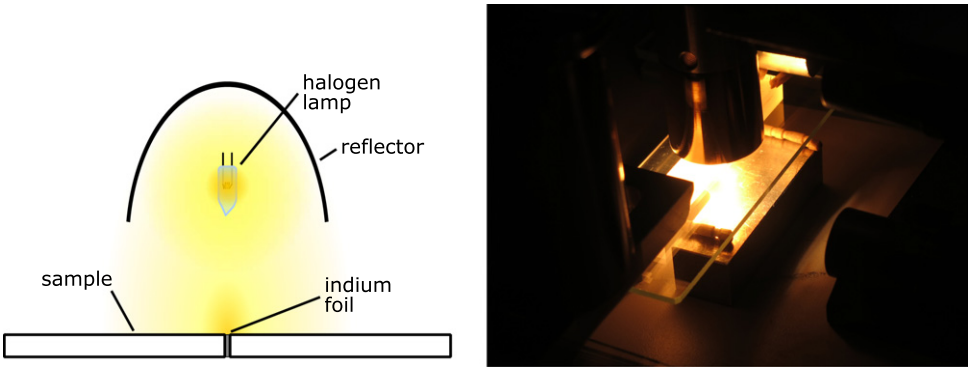

(a) (b)

Figure 4. (a) Schematic drawing of the setup seen in (b) used to prepare the bar samples for the heat extraction measurement. The spot from a halogen lamp (35 W) inside a parabolic reflector was used to heat the indium foil between both sapphire bars.

(95 ± 5) % (see figure 3(b)). Again the thickness of the indium joint was measured and found to be (13.6 ± 2.0) μm.

For the heat removal experiment, two bar samples were joined using a 100 μm thick indium foil. The two samples were placed onto each other with a small external force to keep the samples together. The indium joint region was then heated by means of the radiation of a halogen lamp (see figure 4). Thus a joint of (77.4 ± 2.0) μm was measured as described above. After measuring, the joint was separated which allowed a visual inspection of the

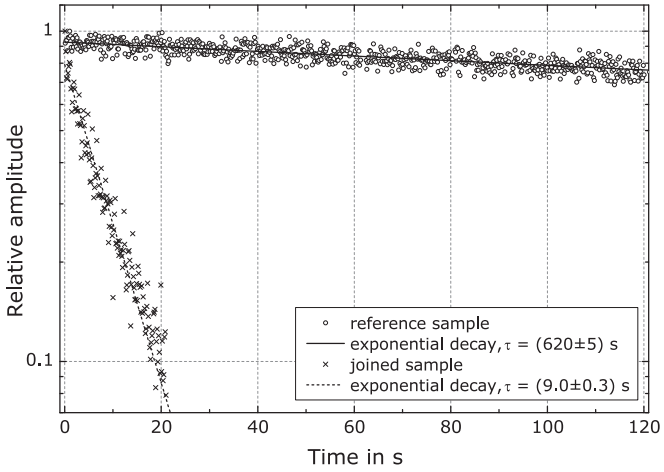

Figure 5. Measured exponential decay of the amplitude of a resonant vibration at 17.2 kHz of the reference sample and the sample joined by the compact indium layer both at a temperature of roughly 6.5 K. While for the reference sample (open circles) the amplitude slowly decreases with time (solid line, $\tau = (620 \pm 5)\,s$) the joined sample (crosses) exhibits a fast decay within a few seconds (dashed line, $\tau = (9.0 \pm 0.3)\,s$) and thus stronger damping.

dense indium layer to take place (see figure 8) as well as allowing it to be peeled it off to measure its weight of (0.015 ± 0.001) g for comparison. The thickness was calculated to be $(82 \pm 22)\,\mu$m (for $\rho = 7310\,\mathrm{kg\,m^{-3}}$) which is in good agreement with the previous result.

The thicker indium film was suitable for the heat removal measurement, as discussed in section 4.

3. Mechanical loss of indium joints

The mechanical loss ϕ serves as a measure of the dissipation of vibrational energy in a system [59] and is defined as the ratio of dissipated energy ΔE per cycle to the maximum of the elastic energy E_{tot}:

$$\phi = \frac{\Delta E}{2\pi E_{\mathrm{tot}}}. \tag{1}$$

It can be obtained by recording the specimen's free ring down of its resonant vibrations which are typically in the kHz range. For that purpose the cylinder-shaped samples were suspended using a single loop of 35 μm thin tungsten wire around their circumference. The samples then were excited to resonant mechanical vibrations by an electrical field of a driving plate. The plate is placed 1 mm from the sample and driven by an amplifier and a frequency generator providing up to 1.6 kV in a frequency range from several kHz to a few hundred kHz . The mechanical vibrations are read out by a laser vibrometer and acquired via LabView. Further details of the setup can be found in [60].

While scanning the excitation frequency, the resonant vibration at f_0 is reached. The excitation is switched off and the amplitude decays exponentially with the ring down time τ starting at an initial amplitude of A_0:

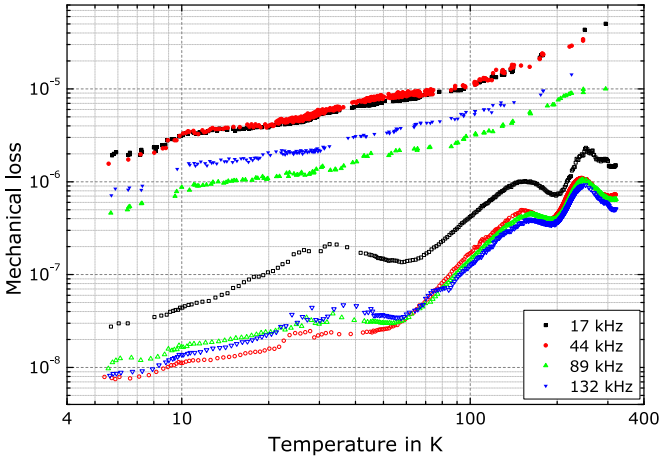

Figure 6. The mechanical loss of the joined sample (solid symbols) is at least one order of magnitude higher compared to that of the reference sample (open symbols). For convenience, only the measurement of the sample joined by the compact indium layer is shown.

$$A(t) = A_0 \exp(-t/\tau). \tag{2}$$

Then the mechanical loss of the system is given by $\phi^{-1} = \pi f_0 \tau$. Figure 5 compares two ring downs of the indium joint and a reference sample at nearly the same frequency. It can be seen that the ring-down time of the joined sample is much shorter than the one of the reference sample. Thus, the mechanical loss of the joined sample is much higher than that of the reference sample.

The measurement of the mechanical loss has been repeated at different resonant modes from 17 kHz to 132 kHz and at different temperatures in a range from 5 K to 300 K. These measurements have been repeated with the reference sample for comparison. The results are summarized in figure 6.

Using (1) we can find the dissipated energy per cycle ΔE which consists of the energy dissipation by the sapphire substrate ΔE_{sub} and additionally by the indium layer $\Delta E_{\mathrm{layer}}$. Thus the measured mechanical loss ϕ_{meas} follows as

$$\phi_{\mathrm{meas}} = \frac{\Delta E_{\mathrm{sub}} + \Delta E_{\mathrm{layer}}}{2\pi E_{\mathrm{tot}}} = \frac{\Delta E_{\mathrm{sub}}}{2\pi E_{\mathrm{sub}}} \frac{E_{\mathrm{sub}}}{E_{\mathrm{tot}}} + \frac{\Delta E_{\mathrm{layer}}}{2\pi E_{\mathrm{layer}}} \frac{E_{\mathrm{layer}}}{E_{\mathrm{tot}}} \tag{3}$$

$$= \phi_{\mathrm{sub}} \frac{E_{\mathrm{sub}}}{E_{\mathrm{tot}}} + \phi_{\mathrm{layer}} \frac{E_{\mathrm{layer}}}{E_{\mathrm{tot}}} \tag{4}$$

and one can find

$$\phi_{\mathrm{meas}} E_{\mathrm{tot}} = \phi_{\mathrm{sub}} E_{\mathrm{sub}} + \phi_{\mathrm{layer}} E_{\mathrm{layer}}. \tag{5}$$

As the indium layer is small compared to the sapphire, most of the energy is stored in the sapphire rather than in the indium layer and we have $E_{\mathrm{tot}} \approx \mathrm{E}_{\mathrm{sub}}$. Further, the mechanical loss of the single piece of sapphire was measured to be at least one order of magnitude lower than that of the joined sample $\phi_{\mathrm{sub}} \ll \phi_{\mathrm{meas}}$ (see figure 6). This allows us to make the following assumption:

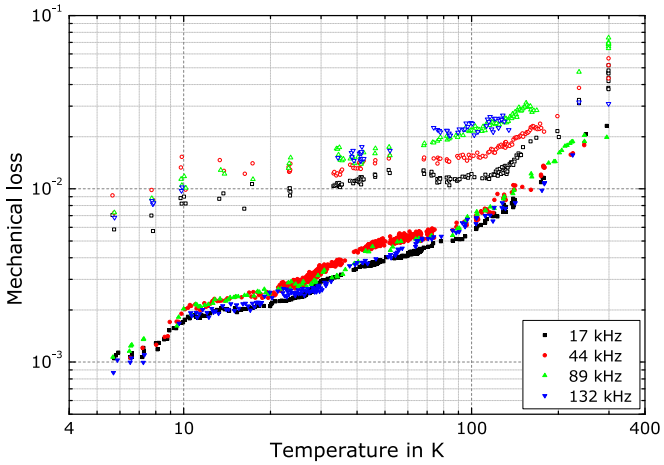

Figure 7. The extracted mechanical loss of both the compact (solid symbols) and the porous (open symbols) indium layers is shown. The loss decreases with decreasing temperature but is always lower for the compact layer which reaches a range of 2×10^{-3} to 3×10^{-3} at 20 K. At this temperature the loss of the porous layer is five times higher.

$$\phi_{\text{meas}} \approx \phi_{\text{layer}} \frac{E_{\text{layer}}}{E_{\text{tot}}} \quad \rightarrow \quad \phi_{\text{layer}} \approx \phi_{\text{meas}} \frac{E_{\text{tot}}}{E_{\text{layer}}}. \tag{6}$$

Thus to extract the mechanical loss of the pure indium layer from the measured data the ratio of elastic energy stored in the whole sample, E_{tot}, to that in the layer, E_{layer}, is needed. Therefore a numerical calculation using the finite element analysis Comsol[8] was used. All necessary material parameters, as well as temperature dependence, can be found in appendix B.

When building models for finite element analysis it is necessary to set up a convenient mesh, especially in this case where two big cylinders of 30 mm diameter and lengths of 50 mm and 70 mm, respectively, are joined by an intermediate layer of only a few μm thickness. One way to overcome this problem is to start with a thicker layer in the mm range of the model. In a similar manner the energy ratio was calculated for a stepwise decreased thickness. Considering the overall deformation of the thin layer, a nearly linear relation of the stored elastic energy in the layer E_{layer} on its thickness t_{layer} is expected. This assumption still holds when the layer thickness becomes more and more reduced. It is also clear that $E_{\text{layer}} = 0$ for a vanishing layer ($t_{\text{layer}} = 0$).

An alternative approach is adopted from [61]. Some assumptions can be made regarding the elastic response of the layer to deformations under resonant vibrations of the whole sample. Deformations u and v of the sapphire surfaces parallel to the layer are carried forward directly to the indium. Also, forces acting perpendicular to the surface F_z stay the same when changing from sapphire to indium. This allows the assumption that all stresses σ_{ij} perpendicular as well as all strains ε_{ij} parallel to the layer to be equal in both sapphire and indium. Then the remaining stresses and strains of the indium at the boundary can be calculated [62]. Due to the small thickness of the layer, these values can be assumed to be constant through the whole layer. Thus the stored elastic energy per layer thickness by the integral over the

[8] https://www.comsol.de/

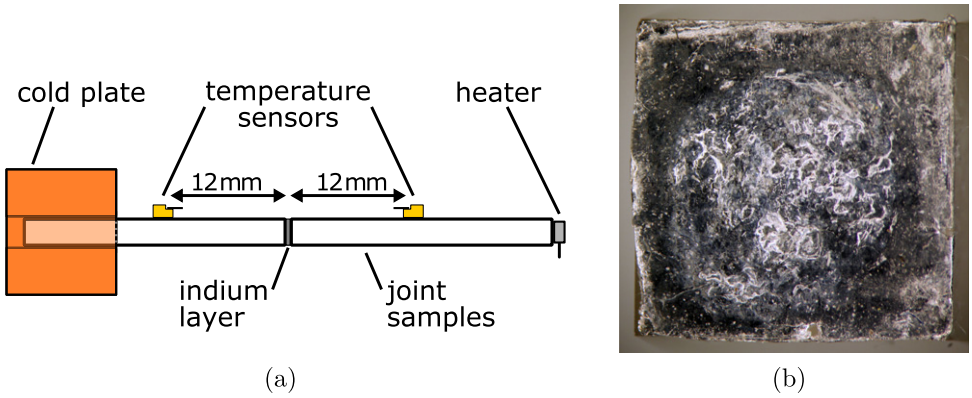

Figure 8. (a) Heat extraction setup. One end of the joined samples is attached to a temperature controlled cold plate while the other end is heated. The temperature difference across the indium layer is recorded by two temperature sensors. (b) Photograph of the indium layer between the bar samples after separation. The layer was revealed to be compact over the whole crossectional area.

boundary surface A reads:

$$\frac{E_{\text{layer}}}{t_{\text{layer}}} = \int_A \frac{1}{2}\sigma'_{ij}\epsilon'_{ij}d^2r. \tag{7}$$

For both of the above approximations the results of E_{tot} and E_{layer} are consistent. Thus the finite element analysis together with the measured thickness serves to extract the mechanical loss of the indium layer in this measurement.

Figure 7 summarizes the extracted mechanical loss of the indium joint for different frequencies and at different temperatures. The measured losses for the porous indium layer are about a factor of ten larger than those for the compact indium layer. This can be correlated with intrinsic friction effects within the porous film. The compact layer resulted in mechanical losses of about 2×10^{-3} to 3×10^{-3} at 20 K. Within the errors of the measurement these values can be considered to be frequency independent.

4. Heat flow through indium joints

Besides low mechanical loss—and thus low thermal noise—the indium joint needs to fulfil a second task: it needs to be able to extract the residual heat in the mirror which originates from optical absorption. The cold side of the suspension fibre is kept at 16 K by means of a cold link to the cryocooler system [23, 63]. The mirror side of the suspension should achieve a minimum temperature of 20 to 24 K during full optical power operation. The suspension fibres under discussion have been proven to provide enough cooling power [64].

Two sapphire pieces have been joined by means of indium as described in section 2.3 in order to check the heat extraction behaviour. The sample had an indium thickness of (77.4 $\pm$ 2.0) μm.

A schematic view of the setup and its realization can be found in figure 8(a). One end of the sample was mounted onto a temperature controlled cold plate inside a cryostat. Two calibrated temperature sensors (Lakeshore DT-670) were attached on both sides, 12 mm away from the joint. At the free end of the sample a resistive heater was attached, with a resistance

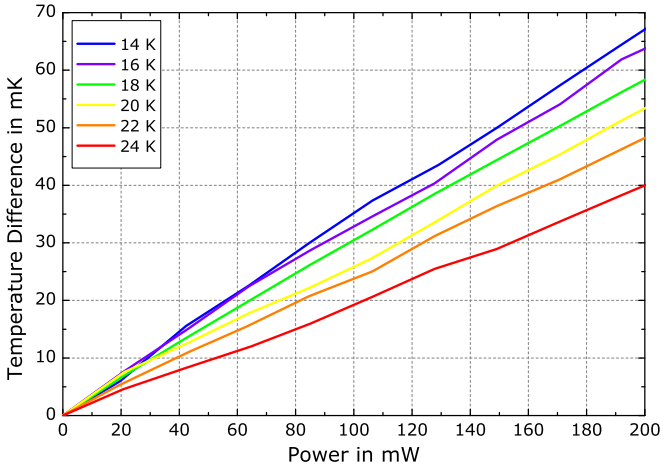

Figure 9. Temperature difference between two points which are 12 mm away from the indium joint, each at different heating powers and temperatures. In KAGRA 140 mW of heat needs to be extracted through an indium layer with a cross section of 350 mm^2 which corresponds to a power of 10 mW in our experiment with a 25 mm^2 cross section. This results in a temperature difference of less than 5 mK.

of 100 Ω. The whole setup was enclosed by means of a heat shield that was kept to the average sample temperature in order to minimize heat radiation from the sample. Details of the setup can be found in [64].

After the desired temperature was reached at the cold plate and the sample different heating powers were applied to the sample, the temperatures at both sides of the indium joint were measured. The temperature difference between these two points is plotted against the heating power in figure 9 for the relevant temperature range of 16 to 24 K.

With increasing the heating power, the temperature difference between the two sensors increases as expected. At lower temperatures this temperature difference is bigger at a given heating power. At a given constant temperature difference, more heat gets extracted in the case of higher sample temperatures. Compared to a pure sapphire sample with the same geometry, the extractable heat is reduced by means of the thin indium layer. For example, the maximum temperature difference at 20 K with a pure sapphire sample in the same geometry would be around 10 mK at a heat flux of 200 mW.

5. Implications for the KAGRA detector

In order to give a first estimate of the thermal noise performance of a cryogenic suspension which uses indium as its jointing material, a finite element analysis was carried out [65]. Following [66] a Gaussian pressure distribution with a sinusoidal oscillation with a frequency $\omega/2\pi$ was applied to a test mass model which contained the test mass as well as the relevant suspension elements. The total thermal noise read out by the laser beam at a temperature T is given by

$$S_{\hat{x}}(\omega, T) = \frac{8k_B T}{\omega^2}\frac{W_{\mathrm{diss}}}{F_0^2} \tag{8}$$

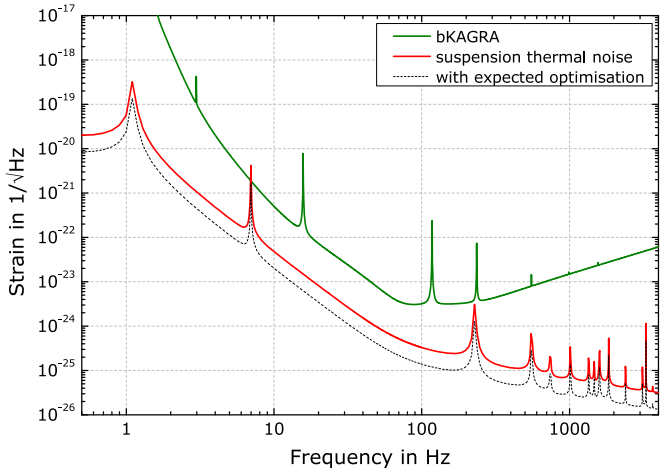

Figure 10. The suspension thermal noise estimate calculated with a loss of 3×10^3 for the indium joints (red curve) is well below the requirements for bKAGRA (green curve). Further improvement is expected (dashed black curve), as explained in the text.

with F_0 being the maximum pressure applied to the surface and W_{diss} the dissipated mechanical energy under this external oscillation. The dissipated mechanical energy is given by

$$W_{\mathrm{diss}} = \omega \int \epsilon\,(x,\,y,\,z)\,\phi\,(x,\,y,\,z)\mathrm{d}^3 r \tag{9}$$

in the case of structural losses which are homogeneously distributed $\phi(x,\,y,\,z)$ [66]. The mechanical energy density $\epsilon(x,\,y,\,z)$ is obtained from a finite element analysis using Ansys[9] or Comsol. The mechanical loss ϕ is taken from the investigations above in the case of indium and from [67] and our reference measurements for the sapphire components. First results of the intrinsic loss of a hydroxide catalysis bond between sapphire pieces have been reported in [68]. Further details of the thermal noise analysis can be found in [65].

Figure 10 compares the obtained thermal noise level with the design goal for KAGRA. It can be seen that the mechanical losses obtained for the indium joints presented in this paper are sufficiently low to achieve the KAGRA thermal noise goals. Additionally, investigations of better indium layers fabricated by means of thermal evaporation have been reported [69]. Here, mechanical losses as low as 4×10^{-4} could be achieved at 20 K which leads to a further reduction in thermal noise as shown in figure 10. However, this procedure is currently not available for a full-sized test mass and suspension for KAGRA and should be seen as a potential path for the future if the process of indium joints can be improved.

In the case of KAGRA, a total heating power of 550 mW needs to be extracted via four crystalline sapphire fibres [64] in the case of the input test mass. This corresponds to about 140 mW per fibre. A much smaller heat load will be experienced by the end test mass as no transmission through the bulk material occurs. The upper end of the fibre is kept at 16 K and the lower end should supply about 20 K operational temperature for the optical component. The sapphire fibres for KAGRA are equipped with square end pieces which are used for the necessary attachments. Thus, the cross section of the indium interface at these end pieces is approximately 350 mm^2 for the upper attachment as well as the lower attachment to the test

[9] http://www.ansys.com/

mass. The increased interface area of the indium joint, as compared to the fibre cross section, converts the 140 mW that needs to be extracted to a 25 mm^2 equivalent of 10 mW. Measurements presented in figure 9 reveal that such a small heat flux through the indium joint will only cause an additional increase of temperature of about 10 mK for two joints per fibre. Compared to the temperature difference of 4 K between the upper and lower end of the fibre, this 10 mK can clearly be tolerated for KAGRA. Although these values are based on a rather thick layer of indium it can be taken as an upper limit. A thinner indium layer is expected to have at worst no larger thermal resistance than a thick layer. In the case that the dominating thermal resistance occurs from the interface between sapphire and indium, the overall thermal resistance would be independent of the thickness. If the main contribution arises from the indium material itself, a thinner indium layer would lead to a better thermal conductivity of the interface and thus even better values than those discussed here.

6. Summary

We investigated a jointing technique for cryogenic sapphire suspensions for KAGRA. The technique utilizes thin indium foil placed between the parts to be joined. Subsequent heating above the melting point, of around 156 °C for indium, allows for the formation of a stable joint. A main advantage of these joints is the ease of disassembling in case of a failure. The mechanical loss ϕ of the joints was found to be as low as 2×10^{-3} at the desired temperature of 20 K. This ensures a low thermal noise of the suspension system well below the requirements of bKAGRA when indium joints are implemented. Additionally, it was demonstrated that the indium joints presented here are capable of extracting enough heat from the test masses in the KAGRA case. The temperature increase of the test masses is not more than 10 mK due to the heat resistance of the indium joints. In both cases, more investigations are needed in order to understand the origin of the intrinsic loss as well as the thermal resistance of the joint.

Acknowledgments

The authors thank R DeSalvo who introduced indium as a jointing material in the Kagra project in 2012.

This collaborative work was done under the Marie Curie program PEOPLE-IRSES (GA 295153). The support of the German Science Foundation under contract SFB TR7 is gratefully acknowledged. The authors would also like to thank the Science and Technology Facilities Council (STFC, grant number ST/L000946/1 'Investigations in Gravitational Research') as well as the Japanese Society for Promotion of Science (JSPS) for their support. This work was supported by MEXT, Leading-Edge Research Infrastructure Program, JSPS Grant-in-Aid for Specially Promoted Research 26000005, and JSPS Core-to-Core Program, A. Advanced Research Networks.

This document has the LIGO document number LIGO-P1500081 and JGW document number JGW-T1503667.

Appendix A. Boundary conditions used for the extraction of the indium layer mechanical loss

The boundary conditions in terms of stresses σ_{ij} and strains ε_{ij} are as follows:

$$\begin{aligned}
\sigma'_{xz} &= \sigma_{xz} \qquad & \varepsilon'_{xx} &= \varepsilon_{xx} \\
\sigma'_{yz} &= \sigma_{yz} \qquad & \varepsilon'_{yy} &= \varepsilon_{yy} \\
\sigma'_{zz} &= \sigma_{zz} \qquad & \varepsilon'_{xy} &= \varepsilon_{xy}
\end{aligned}$$

where the primed values denote properties of the indium layer and the unprimed ones correspond to sapphire. Following [62], the missing components are given by:

$$\begin{aligned}
\sigma'_{xx} &= \frac{Y'}{\left(1+\nu'\right)\left(1-2\nu'\right)}\left[\left(1-\nu'\right)\varepsilon'_{xx} + \nu'\left(\epsilon'_{yy} + \varepsilon'_{zz}\right)\right] \\
\sigma'_{yy} &= \frac{Y'}{\left(1+\nu'\right)\left(1-2\nu'\right)}\left[\left(1-\nu'\right)\varepsilon'_{yy} + \nu'\left(\epsilon'_{xx} + \varepsilon'_{zz}\right)\right] \\
\sigma'_{xy} &= \frac{Y'}{1+\nu'}\varepsilon'_{xy} \\
\varepsilon'_{zz} &= \frac{1}{Y'}\left[\sigma'_{zz} - \nu'\left(\sigma'_{xx} + \sigma'_{yy}\right)\right] \\
\varepsilon'_{xz} &= \frac{1+\nu'}{Y'}\sigma'_{xz} \\
\varepsilon'_{yz} &= \frac{1+\nu'}{Y'}\sigma'_{yz}
\end{aligned}$$

and finally by rearranging:

$$\begin{aligned}
\sigma'_{xx} &= \frac{\sigma'_{zz}\nu'\left(1+\nu'\right) + \left(\epsilon'_{xx} + \epsilon'_{yy}\nu'\right)Y'}{1-\nu'^2} \\
\sigma'_{yy} &= \frac{\sigma'_{zz}\nu'\left(1+\nu'\right) + \left(\epsilon'^{yy} + \epsilon'_{xx}\nu'\right)Y'}{1-\nu'^2} \\
\varepsilon'_{zz} &= \frac{\sigma'_{zz}\left(1-\nu'-2\nu'^2\right) - \left(\epsilon'_{xx} + \epsilon'_{yy}\right)\nu'Y'}{\left(1-\nu'\right)Y'}.
\end{aligned}$$

Further, due to the small thickness of the layer, these values are assumed to be constant along the z-axis. Thus the stored elastic energy per layer thickness is given by the integral over the jointing surface A:

$$\frac{E_{\text{layer}}}{t_{\text{layer}}} = \int_A \frac{1}{2}\sigma'_{ij}\epsilon'_{ij}\mathrm{d}^2r.$$

Appendix B. Material parameters and their temperature dependence

Sapphire: the elastic constants C_{ij} of sapphire show hardly any dependence on temperature and thus were assumed constant in the temperature region considered. The values are taken from [70] at 296 K and given in Voigt notation:

$$C_{11} = 497.3\ \text{GPa} \qquad C_{12} = 162.8\ \text{GPa}$$
$$C_{33} = 500.9\ \text{GPa} \qquad C_{13} = 116.0\ \text{GPa}$$
$$C_{44} = 146.8\ \text{GPa} \qquad C_{14} = 21.9\ \text{GPa}$$

Indium: the Young's modulus of polycrystalline indium increases by nearly a factor of two when cooled down to 5 K. The Poisson's ratio changes by just four percent. Elastic constants of indium can be found from [71]. At room temperature the Young's modulus is 12.74 GPa and the Poisson's ratio equals 0.4498. The temperature dependence can be found in [71] and is given by the equations:

$$Y(T) = 12.74\ \text{GPa} \times \left(1.536 - \frac{0.1814}{\exp(86.02\ K/T) - 1}\right)$$
$$\nu(T) = 0.4498 \times \left(0.9574 - \frac{-0.01518}{\exp(90.83\ K/T) - 1}\right).$$

Appendix C. RCA standard clean

The RCA standard clean [58] applied to the samples consists of two solutions named SC-1 and SC-2. SC-1 is made of hydrogen peroxide (H_2O_2, 30%) and ammonium hydroxide (NH_4OH, 25%) one part each mixed with five parts of deionised water (H_2O). The second mixture, SC-2, again uses the same amounts of hydrogen peroxide and hydrogen chloride (HCl 37%) diluted by six amounts of deionised water. Both solutions were heated to 75 °C to 80 °C prior to use.

The samples are rinsed with deionised water, then put into SC-1 and kept inside an ultrasonic bath for 10 min. Afterwards they are rinsed again with deionised water before the procedure is repeated using the SC-2 solution. The samples are given a final rinse in deionised water and are blown dry by high purity nitrogen.

References

[1] Abbott B P *et al* 2009 Advance LIGO: The Laser interferometer gravitational-wave observatory *Rep. Prog. Phys.* **72** 076901
[2] The LIGO Scientific Collaboration 2015 Advanced LIGO *Class. Quantum Grav.* **32** 074001
[3] Accadia T *et al* 2012 Virgo: a laser interferometer to detect gravitational waves *J. Instrum.* **7** P03012
[4] Grote H and LIGO Scientific Collaboration 2010 The GEO 600 status *Class. Quantum Grav.* **27** 084003
[5] Abadie J *et al* 2011 Beating the spin-down limit on gravitational wave emission from the Vela Pulsar *Astrophys. J.* **737** 93
[6] Abadie J *et al* 2012 All-sky search for gravitational-wave bursts in the second joint LIGO-Virgo run *Phys. Rev.* D **85** 122007
[7] Abadie J *et al* 2012 Search for gravitational waves from low mass compact binary coalescence in LIGO's 6th science run and Virgo's science runs 2 and 3 *Phys. Rev.* D **85** 082002
[8] Aasi J *et al* 2014 Gravitational waves from known pulsars: Results from the initial detector era *Astrophys. J.* **785** 119
[9] Aasi J *et al* 2014 Improved upper limits on the stochastic gravitational-wave background from 2009-2010 LIGO and Virgo data *Phys. Rev. Lett.* **113** 231101
[10] Acernese F *et al* 2015 Advanced Virgo: a second-generation interferometric gravitational wave detector *Class. Quantum Grav.* **32** 024001

[11] Plissi M V, Strain K A, Torrie C I, Robertson N A, Killbourn S, Rowan S, Twyford S M, Ward H, Skeldon K D and Hough J 1998 Aspects of the suspension system for GEO 600 *Rev. Sci. Instrum.* **69** 3055–61
[12] Harry G, Corbitt T, Freytsis M, Ottaway D, Mavalvala N and Penn S 2006 Mechanical loss of laser-welded fused silica fibers *Rev. Sci. Instr.* **77** 023906
[13] Heptonstall A *et al* 2010 Investigation of mechanical dissipation in Co_2 laser-drawn fused silica fibres and welds *Class. Quantum Grav.* **27** 035013
[14] Rowan S, Twyford S M, Hough J, Gwo D-H and Route R 1998 Mechanical losses associated with the technique of hydroxide-catalysis bonding of fused silica *Phys. Lett.* A **246** 471–8
[15] Meers B J 1988 Recycling in laser-interferometric gravitational-wave detectors *Phys. Rev.* D **38** 2317–26
[16] Strain K A *et al* 2003 Sensing and control in dual-recycling laser interferometer gravitational-wave detectors *Appl. Opt.* **42** 1244–56
[17] Kwee P *et al* 2012 Stabilized high-power laser system for the gravitational wave detector advanced ligo *Opt. Express* **20** 10617–34
[18] The LIGO Scientific Collaboration 2011 A gravitational wave observatory operating beyond the quantum shot-noise limit *Nat. Phys.* **7** 962–5
[19] Affeldt C *et al* 2014 Advanced techniques in GEO 600 *Class. Quantum Grav.* **31** 224002
[20] Smith J R, Cagnoli G, Crooks D R M, Fejer M M, Gossler S, Lück H, Rowan S and Hough Jand Danzmann K 2004 Mechanical quality factor measurements of monolithically suspended fused silica test masses of the GEO 600 gravitational wave detector *Class. Quantum Grav.* **21** S1091
[21] Grote H, Danzmann K, Dooley K L, Schnabel R, Slutsky J and Vahlbruch H 2013 First long-term application of squeezed states of light in a gravitational-wave observatory *Phys. Rev. Lett.* **110** 181101
[22] Kuroda K and LCGT Collaboration 2010 Status of LCGT *Class. Quantum Grav.* **27** 084004
[23] Kentaro S 2012 Detector configuration of KAGRA—the Japanese cryogenic gravitational-wave detector *Class. Quantum Grav.* **29** 124007
[24] Hirose E, Sekiguchi T, Kumar R, Takahashi R and for the KAGRA collaboration 2014 Update on the development of cryogenic sapphire mirrors and their seismic attenuation system for KAGRA *Class. Quantum Grav.* **31** 224004
[25] Rowan S, Hough J and Crooks D R M 2005 Thermal noise and material issues for gravitational wave detectors *Phys. Lett.* A **347** 25–32
[26] Nawrodt R, Rowan S, Hough J, Punturo M, Ricci F and Vinet J-Y 2011 Challenges in thermal noise for 3rd generation of gravitational wave detectors *Gen. Relativ. Gravit.* **43** 593–622
[27] Tomaru T, Suzuki T, Miyoki S, Uchiyama T, Taylor C T, Yamamoto A, Shintomi T, Ohashi M and Kuroda K 2002 Thermal lensing in cryogenic sapphire substrates *Class. Quantum Grav.* **19** 2045
[28] McSkimin H J 1953 Measurement of elastic constants at low temperatures by means of ultrasonic waves-data for silicon and germanium single crystals, and for fused silica *J. Appl. Phys.* **24** 988–97
[29] Marx J W and Sivertsen J M 1953 Temperature dependence of the elastic moduli and internal friction of silica and glass *J. Appl. Phys.* **24** 81–7
[30] Fine M E, Van Duyne H and Kenney N T 1954 Low temperature internal friction and elasticity effects in vitreous silica *J. Appl. Phys.* **25** 402–5
[31] Anderson O L and BÖmmel H E 1955 Ultrasonic absorption in fused silica at low temperatures and high frequencies *J. Am. Ceram. Soc.* **38** 125–31
[32] Kittel C 1949 Interpretation of the thermal conductivity of glasses *Phys. Rev.* **75** 972
[33] Cahill D G and Pohl R O 1987 Thermal conductivity of amorphous solids above the plateau *Phys. Rev.* B **35** 4067–73
[34] Winkler W, Danzmann K, Rüdiger A and Schilling R 1991 Heating by optical absorption and the performance of interferometric gravitational-wave detectors *Phys. Rev.* A **44** 7022–36
[35] Ju L, Notcutt M, Blair D, Bondu F and Zhao C N 1996 Sapphire beamsplitters and test masses for advanced laser interferometer gravitational wave detectors *Phys. Lett.* A **218** 197–206
[36] Uchiyama T *et al* 1999 Mechanical quality factor of a cryogenic sapphire test mass for gravitational wave detectors *Phys. Lett.* A **261** 5–11
[37] Tomaru T, Uchiyama T, Tatsumi D, Miyoki S, Ohashi M, Kuroda K, Suzuki T, Yamamoto A and Shintomi T 2001 Cryogenic measurement of the optical absorption coefficient in sapphire

crystals at 1.064 μm for the large-scale cryogenic gravitational wave telescope *Phys. Lett.* A **283** 80–4
[38] Amico P, Bosi L, Carbone L, Gammaitoni L, Marchesoni F, Punturo M, Travasso F and Vocca H 2002 Mechanical quality factor of large mirror substrates for gravitational waves detectors *Rev. Sci. Instrum.* **73** 179–84
[39] Nawrodt R, Zimmer A, Koettig T, Nietzsche S, Thürk M, Vodel W and Seidel P 2007 High mechanical Q-factor measurements on calcium fluoride at cryogenic temperatures *Eur. Phys. J. Appl. Phys.* **38** 53–9
[40] Schwarz C, Heinert D, Seidel P, Tünnermann A, Hammond G D and Nawrodt R 2011 Mechanical loss of calcium fluoride at cryogenic temperatures *Phys. Status Solidi a* **208** 2719–23
[41] Reid S, Cagnoli G, Crooks D R M, Hough J, Murray P G, Rowan S, Fejer M M, Route R and Zappe S 2006 Mechanical dissipation in silicon flexures *Phys. Lett.* A **351** 205–11
[42] Nawrodt R *et al* 2008 High mechanical Q-factor measurements on silicon bulk samples *J. Phys.: Conf. Ser.* **122** 012008
[43] Nawrodt R *et al* 2013 Investigation of mechanical losses of thin silicon flexures at low temperatures *Class. Quantum Grav.* **30** 115008
[44] Punturo M *et al* 2010 The Einstein Telescope: a third-generation gravitational wave observatory *Class. Quantum Grav.* **27** 194002
[45] Suzuki T *et al* 2006 Application of sapphire bonding for suspension of cryogenic mirrors *J. Phys.: Conf. Ser.* **32** 309
[46] Dari A, Travasso F, Vocca H and Gammaitoni L 2010 Breaking strength tests on silicon and sapphire bondings for gravitational wave detectors *Class. Quantum Grav.* **27** 045010
[47] Douglas R, van Veggel A A, Cunningham L, Haughian K, Hough J and Rowan S 2014 Cryogenic and room temperature strength of sapphire jointed by hydroxide-catalysis bonding *Class. Quantum Grav.* **31** 045001
[48] Haughian K, Douglas R, van Veggel A A, Hough J, Khalaidovski A, Rowan S, Suzuki T and Yamamoto K 2015 The effect of crystal orientation on the cryogenic strength of hydroxide catalysis bonded sapphire *Class. Quantum Grav.* **32** 075013
[49] Gwo D 1998 Ultra-precision bonding for cryogenic fused-silica optics *Proc. SPIE* **3435** 136–42
[50] Cunningham L *et al* 2010 Re-evaluation of the mechanical loss factor of hydroxide-catalysis bonds and its significance for the next generation of gravitational wave detectors *Phys. Lett.* A **374** 3993–8
[51] Lorenzini M 2010 and the Virgo Collaboration, The monolithic suspension for the Virgo interferometer *Class. Quantum Grav.* **27** 084021
[52] Cumming A V *et al* 2012 Design and development of the advanced LIGO monolithic fused silica suspension *Class. Quantum Grav.* **29** 035003
[53] Twyford S M 1998 Developments towards low loss suspensions for laser interferometric gravitational wave detectors *PhD Thesis* University of Glasgow
[54] See e.g. KAGRA documents jgw-g1201265-v2 or jgw-g1201174-v1 available under http://gwdoc.icrr.u-tokyo.ac.jp/cgi-bin/docdb/documentdatabase.
[55] Straessle R, Pétremand Y, Briand D and de Rooij N F 2011 Evaluation of thin film indium bonding at wafer level *Proc. Eng.* **25** 1493–6
[56] Impex HighTech GmbH.
[57] Kern W and Puotinen D 1970 The RCA-clean *RCA Rev.* **31** 197
[58] Kern W 1990 The evolution of silicon wafer cleaning technology *J. Electrochem. Soc.* **137** 1887–92
[59] Saulson P R 1990 Thermal noise in mechanical experiments *Phys. Rev.* D **42** 2437–45
[60] Nawrodt R, Zimmer A, Nietzsche S, Thürk M, Vodel W and Seidel P 2006 A new apparatus for mechanical Q-factor measurements between 5 and 300 k *Cryogenics* **46** 718–23
[61] Harry G M *et al* 2002 Thermal noise in interferometric gravitational wave detectors due to dielectric optical coatings *Class. Quantum Grav.* **19** 897
[62] Landau L D, Lifshitz E M, Kosevitch A M and Pitaevskiĭ L P 1986 Theory of elasticity *Course of Theoretical Physics* (Oxford: Butterworth-Heinemann)
[63] Sakakibara Y *et al* 2014 Progress on the cryogenic system for the KAGRA cryogenic interferometric gravitational wave telescope *Class. Quantum Grav.* **31** 224003
[64] Khalaidovski A *et al* 2014 Evaluation of heat extraction through sapphire fibers for the GW observatory KAGRA *Class. Quantum Grav.* **31** 105004

[65] Chen D 2015 Study of a cryogenic suspension system for the gravitational wave telescope KAGRA *PhD Thesis* The University of Tokyo
[66] Levin Y 1998 Internal thermal noise in the LIGO test masses: A direct approach *Phys. Rev.* D **57** 659–63
[67] Bagdasarov Kh S, Braginsky V B and Mitrofanov V P 1974 Mechanical dissipation in single-crystal sapphire *Kristallografiya* **19** 883
[68] Haughian K 2015 *Bonding of Sapphire and Silicon, talk at the 3rd ELiTES annual meeting, Tokyo*
[69] Murray P G, Martin I W, Cunningham L, Craig K, Hammond G D, Hofmann G, Hough J, Nawrodt R, Reifert D and Rowan S 2015 Low-temperature mechanical dissipation of thermally evaporated indium film for use in interferometric gravitational wave detectors *Class. Quantum Grav.* **32** 115014
[70] Goto T, Anderson O L, Ohno I and Yamamoto S 1989 Elastic constants of corundum up to 1825 k *J. Geophys. Res.: Solid Earth* **94** 7588–602
[71] Kim S and Ledbetter H 1998 Low-temperature elastic coefficients of polycrystalline indium *Mater. Sci. Eng.* A **252** 139–43